

Defect-Free Palladium Membranes on Porous Stainless-Steel Support

Peter P. Mardilovich, Ying She, and Yi Hua Ma

Dept. of Chemical Engineering, Worcester Polytechnic Institute, Worcester, MA 01609

Min-Hon Rei

China Technical Consulting, Inc., Taipei, Taiwan, R.O.C.

Defect-free Pd membranes were prepared by an electroless plating technique on porous stainless-steel tubes. The effective surface of Pd membranes was up to 75 cm². The helium flux was not detected at room temperature and pressure difference of 3 atm. At 350°C hydrogen permeances of up to 8 m³/(m²·h·atm^{0.5}) were obtained. At a pressure difference of 1 atm and 350°C, selectivity coefficients as high as J(H₂)/J(N₂) = 5,000 were observed. Fluxes of gases, impermeable through the Pd, were quantitatively described as a combination of Knudsen diffusion and viscous flow through the gaps created in the Pd layer at high temperatures. The stability of the prepared membranes at temperatures up to 700°C was investigated. The membranes were stable at 350°C over a period of 1,100 h, with no significant changes in the steady-state hydrogen flux and with a recrystallization texture and aggregation of Pd grains.

Introduction

The development of high-temperature processes and tighter environmental regulations requires utilization of gas separation processes that will provide high fluxes, high selectivity of separation, and the ability to operate at elevated temperatures. Hydrogen separation and purification from a reaction gas mixture is an area of particular interest in this respect. Dense metal membranes are especially well suited for high-temperature hydrogen separations. Palladium and its alloys are the most commonly used materials for the preparation of dense metal membranes because of their high hydrogen permeability and chemical resistance (McBride and McKinley, 1965). Compared with unsupported metal membranes, the development of an asymmetric composite membrane with a porous support and thin Pd or Pd-alloy dense layer would provide both higher transmembrane flux and lower Pd loading in the membrane.

There are several major techniques for the deposition of Pd or its alloys on a support. A spray pyrolysis method was used by Li et al. (1993) to deposit a Pd-Ag alloy on the alumina support. Yan et al. (1994) and Morooka et al. (1995) formed a thin palladium membrane inside the porous wall of an α -alumina support tube by the metal-organic chemical-

vapor deposition (MOCVD) technique by decomposing palladium (II) acetate in argon under reduced pressure. A thin (1–2 μ m) Pd layer was also pyrolytically deposited by the supercritical fluid transport-chemical deposition (SFTCD) method using the metal β -diketonate complex—(2,2,7-trimethyl-3,5-octanedionato) palladium (II) (Hybertson et al., 1991). Ultrathin Pd composite membranes were prepared by the sputter-deposition technique on polymeric membranes (Athayde et al., 1994), porous alumina (Jayaraman et al., 1995a,b), anodic alumina (Konno et al., 1988; Mardilovich et al., 1996a), and Vycor glass (Bryden and Ying, 1995) supports. Gryaznov et al. (1993) prepared Pd and Pd-alloy membranes on polymer membranes, porous stainless steel, and oxide plates by magnetic sputtering. Recently (Peachey et al., 1996), electron-beam evaporation and ion-beam sputtering were used to deposit Pd on the surface of tantalum foil. Some other examples of the application of these techniques, as well as physical vapor deposition and electroplating, were briefly discussed in the review by Shu et al. (1991). The major drawbacks of all these powerful techniques, especially useful for the deposition of alloys, are the low area of the prepared membranes and/or high cost of the necessary equipment. The practical applicability of these techniques may require further investigation.

Correspondence concerning this article should be addressed to Y. H. Ma.

On the other hand, electroless plating appears to be quite attractive due to the possibility of uniform deposition on complex shapes and large substrate areas, hardness of the deposited film, and very simple equipment. Electroless plating has been used to produce Pd or Pd-alloy membranes on a wide variety of supports, which include tantalum and niobium tubes (Buxbaum and Marker, 1993; Buxbaum and Kinney, 1996), porous silver (Govind and Atnoor, 1991), porous glass (Uemiya et al., 1988, 1991a), alumina (Uemiya et al., 1991b; Kikuchi and Uemiya, 1991; Collins and Way, 1993), and porous stainless steel (Shu et al., 1993; Mardilovich et al., 1996b; Yeung et al., 1996). Recently, Yeung and Varma (1995) proposed a method of preparation of Pd-composite membranes by using osmotic pressure for the manipulation of the microstructure, porosity, and thickness of the deposited metal.

The main advantages of porous stainless-steel (PSS) supports over porous ceramics, Vycor glass, Ta, V, and so forth, are the resistance to cracking and the simplicity of module construction. Composite Pd/PSS membranes, welded from both ends with nonporous stainless-steel tubes, can be very easily assembled. Additionally, the thermal expansion coefficient of stainless steel is almost identical to that of palladium, ensuring good mechanical properties of the composite membrane during temperature cycling. The first attempt to use PSS as the support was reported by Shu et al. (1993), using a disk with the geometric area of 2 cm², but permeation data were not reported. Data presented by Yeung et al. (1996) indicated that palladium-PSS composite membranes could give high hydrogen fluxes and selectivities. Their results appear to show that the synthesis procedure based on electroless plating with osmosis gives membranes with higher fluxes and better thermal stability than the conventional electroless plating.

The objective of this study is to investigate factors affecting the preparation of dense, defect-free palladium membranes on porous stainless-steel supports and to study the transport mechanisms through the prepared membranes.

Experimental

Porous stainless-steel support

Porous 316L stainless-steel cups and tubes (OD—15.9 and 12.7 mm; wall thickness—1.6 mm; length—19 and 25 mm for cups and 152 mm for tubes) were purchased from Mott Metallurgical Corporation. According to the manufacturer, the grade of these PSS was 0.5 μ m (95% rejection) with 5 μ m the biggest pore diameter and an average pore diameter of 3 μ m (Mott Metallurgical, 1995). The porosity of PSS was 17%. The PSS cups and tubes were electrically welded to nonporous stainless-steel tubes.

Figure 1 shows the SEM pictures of a typical grade 0.5- μ m PSS. There are a number of holes on the surface with the dimension around 20–30 μ m, as shown in Figure 1a. However, it appears that only the entrance of the pore has such a large size. Below the surface they rapidly became narrower and, in general, the diameter of the real pores does not exceed 8 μ m, as can be seen from the SEM picture of the preliminary polished PSS sample, shown in Figure 1b. The presence of such large and deep holes can be an additional

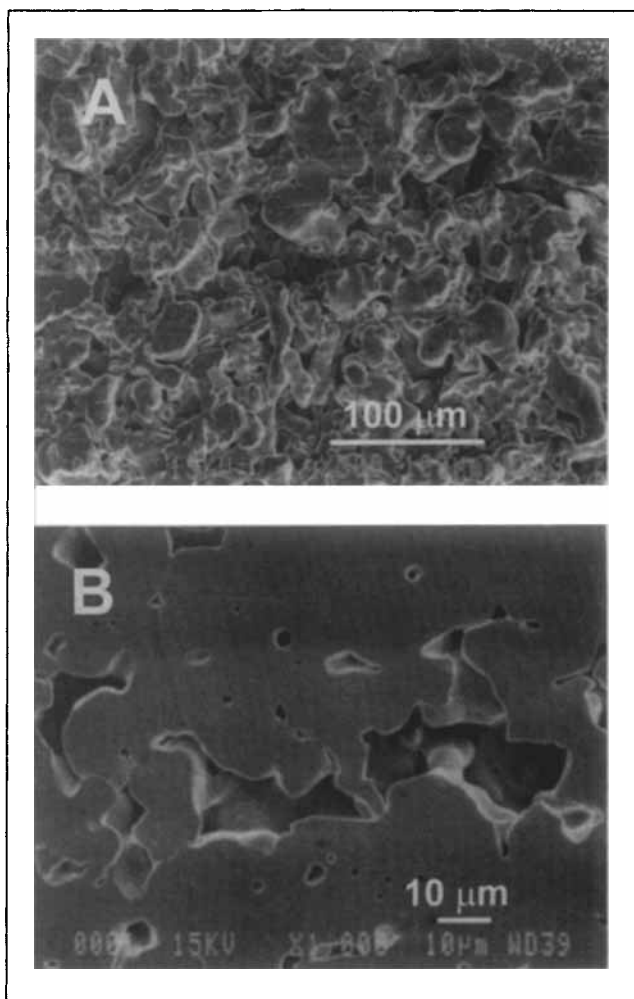


Figure 1. Scanning electron micrographs: (A) original; (B) polished grade 0.5 porous stainless steel.

difficulty in the deposition of the dense palladium layer. On the other hand, these holes, or entrances into the pores, can improve adhesion strength between the Pd film and PSS surface, which depends on the mechanical bonding and the anchoring effects (Honma and Kanemitsu, 1987).

An important characteristic of plating palladium on the PSS is the strength of the bond that can develop between the base stainless steel and the palladium layer. Metal-to-metal bonds with high adhesion values require thorough surface preparation to present a clean and optimally rough surface structure. Foreign contaminants (grease, oil, dirt, corrosion products, and others) should be completely removed from the stainless-steel surface. This was achieved by mechanical treatment (sandpaper, stainless-steel brush, file, etc.) and cleaning the PSS in an ultrasonic bath with alkaline solution at ~60°C followed by rinsing in tap water, deionized water, and isopropanol. The alkaline cleaning solution consisted of a combination of alkaline sodium compounds such as hydroxide, carbonate, phosphate, and organic detergent.

The roughness of the stainless-steel surface was increased by a ~5 min treatment in concentrated hydrochloric acid, followed by water rinsing. Such a treatment also provided the

preactivation of the support surface. The rust on the surface caused by the hydrochloric acid treatment was removed by diluted (~ 40%) phosphoric acid.

Activation

The membranes went through a surface activation prior to the electroless plating. The purpose of the surface activation was to seed the PSS surface with palladium nuclei, which during the electroless plating initiated the autocatalytic process of reducing the metastable Pd salt complex on the target surface. The activation procedure consisted of successive immersions in an acidic SnCl₂ bath (sensitizing) followed by an acidic PdCl₂ bath. After immersion in the SnCl₂ bath, a gentle rinsing with deionized water was used. Rinsing with 0.01 M HCl and then with water was carried out after immersion in the PdCl₂ bath. The 0.01 M HCl solution was used to prevent hydrolysis of Pd²⁺ ions. The typical composition of the activation bath is presented in Table 1.

During rinsing with deionized water after immersion in the acidic SnCl₂ bath, the partial hydrolysis of Sn²⁺ took place to form little (poorly) soluble product, Sn(OH)_{1.5}Cl_{0.5}, and other more complicated hydroxy-chlorides (Melashchenko, 1987). Such tin hydroxy-chlorides were strongly attached to the surface as a layer with a thickness of a thousandth-tenth of a micron. The composition, structure, and thickness of this layer depended on the ratio HCl/SnCl₂, support surface structure, roughness and shape, and the hydrodynamic regime of rinsing.

An excess of Sn²⁺ on the target surface of porous stainless steel can create a loose (crumbly), easy-to-peel layer, while a deficiency of Sn²⁺ can lead to nonuniform seeding of the palladium nuclei. The distribution of catalytic centers for autocatalytic Pd²⁺ reduction must be dense and uniform at an optimum concentration of Sn²⁺ on the surface. To reach this goal, a two-step immersion sequence in SnCl₂ and PdCl₂ solutions was generally repeated 4–10 times, depending on the intensity of the activation. A perfectly activated layer has a uniform dark-brown color and smooth surface. If the quality of the activated layer was unsatisfactory, it was removed in an ultrasonic bath with 1-M HCl and the activation procedure was repeated.

After 10 sensitizing/activation cycles, followed by drying at 120°C for 2 h, the thickness of the activated layer was around 1.5 μm, as can be seen in Figure 2a. The density of the layer, which consisted mainly of Sn(OH)₄ and Pd nuclei, was around 3–3.5 g/cm³. After 5 min treatment by 1-M HCl, the activated layer became fragile, and its porous structure is shown in Figure 2b.

The activation layer can be considered as a sandwich structure consisting of a number of very thin layers, one after each sensitizing/activation cycle, with Pd nuclei on the top of each

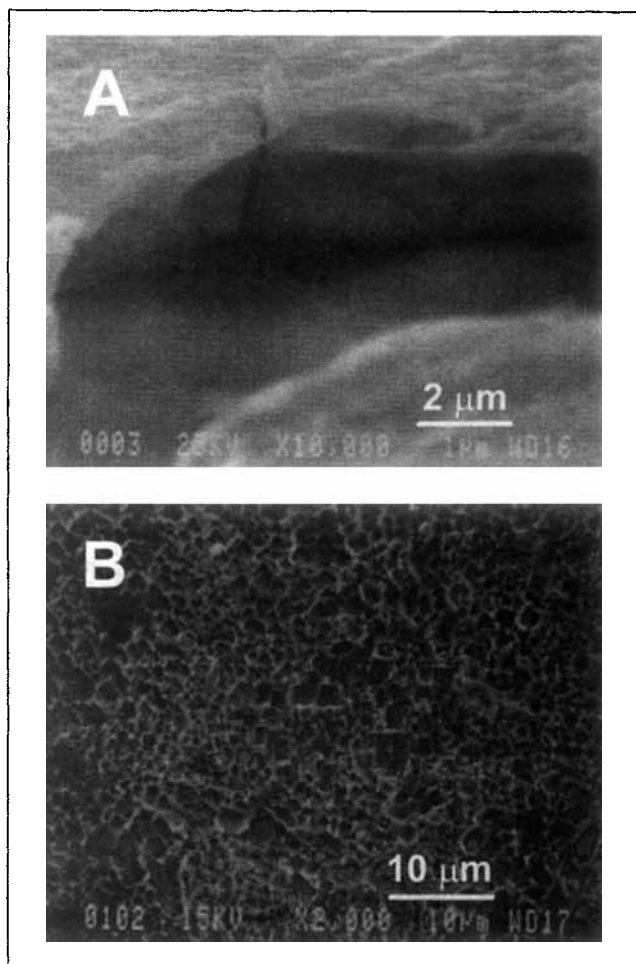
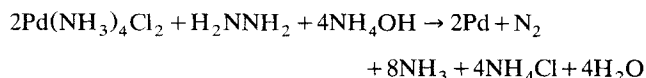


Figure 2. (A) Cross section of activated layer after 10 sensitizing/activation cycles; (B) top view of the partially removed activated layer.

layer. A thicker activated layer results in higher density of Pd nuclei on the support surface, but lowers the adhesion of further deposited Pd layers to the PSS support. In many cases, the optimum activated layer was created after six sensitizing/activation cycles.

Deposition of palladium

Palladium deposition occurs according to the following autocatalytic reaction



or



Preseeded palladium nuclei at the activation stage reduce the induction period of the autocatalytic process at the beginning of the deposition.

Table 1. Composition of the Activation Solutions

	Sn Solution	Pd Solution
SnCl ₂ · 2H ₂ O, g/L	1.0	—
PdCl ₂ , g/L	—	0.1
HCl (~ 37%), ml/L	1	1
Temperature, °C	20°C	20°C
Duration, min	5	3–5

Table 2. Composition of the Electroless Palladium-Plating Bath

Pd(NH ₃) ₄ Cl ₂ · H ₂ O, g/L	4.0
NH ₄ OH (28%), mL/L	198
Na ₂ EDTA, g/L	40.1
H ₂ NNH ₂ (1 M), mL/L	5.6–7.6
pH	~10.4
Temperature, °C	60
$V_{\text{solution}}/S_{\text{plating area}}$, cm ³ /cm ²	~3.5

Table 2 shows a typical plating bath composition. Palladium was deposited on PSS cups by suspending the cups in an electroless-plating bath surrounded by a water jacket for temperature control. For the deposition of palladium on the long tube support a special electroless-plating cell was used. The bath used for the deposition on long tubes is presented in Figure 3. A uniform deposition of Pd on the PSS long tube was achieved by controlled rotation of the support.

The designed cell also allowed for the control of the rate of deposition. The flow of the gases evolved from this reaction was quantitatively measured by a soap-bubble flowmeter. The main component of the gas product was nitrogen. The majority of NH₃, which was a product of the decomposition of palladium tetrammine dichloride, was dissolved in the plating solution. The rest of the ammonia was removed by bubbling the gas through the 1-M HCl solution. Figure 4 shows the nitrogen flow rates for two successive platings

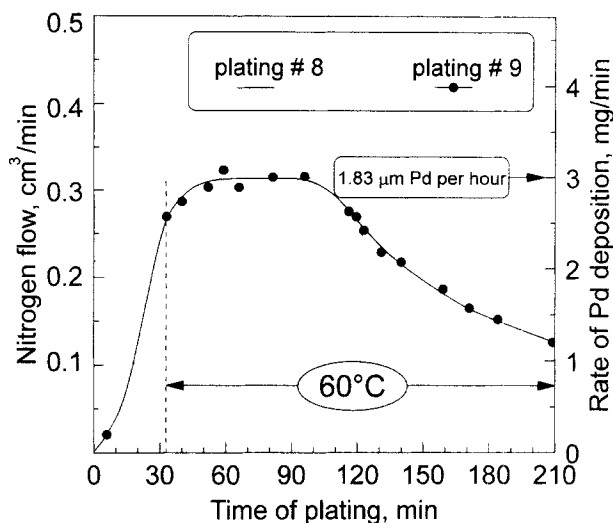


Figure 4. Variation of the nitrogen flow and rate of the palladium deposition with time of plating for two successive plating procedures.

(plating #8 and plating #9). The right axis presents the corresponding rate of the Pd deposition, which was estimated based on the ratio 2Pd/N₂. The increase of the deposition rate during the first 30 min was caused by the changes of bath's temperature from 20°C to 60°C. After approximately one hour of steady-state deposition the activity of the plating decreased with the depletion of palladium ions, hydrazine, and the pH of the plating bath. A stable high rate of deposition for each plating was achieved by carefully rinsing the membrane between plating solutions. There is an excellent agreement between the quantity of the deposited palladium determined by the gas-flow measurement and the integration of these data, and by weighing of the support before and after the deposition.

The thickness of the Pd layer was determined from the plated amount and the density of Pd (12.0 g/cm³). In some cases the thickness was estimated directly from the SEM picture. A total of eight membranes have been prepared and used for the various tests.

Permeation experiments

The permeation measurements of the initial PSS support and the membrane after deposition of the palladium layer were carried out using a stainless-steel membrane assembly. Figure 5 shows the experimental setup. The feed gas flowed upward through the outside of the membrane (shell side), and the permeant gas was collected on the tube side. A purge gas could also be used on the tube side, if desired. The upstream pressure was monitored by a capacitance pressure transducer and the permeate-side pressure was kept atmospheric. The gas permeation rate (the volumetric flow rate) was measured in the permeate side at atmospheric pressure and room temperature. A soap-bubble capillary flowmeter was used for flow rates less than 1 cm³/min; a digital flowmeter (Alltech), for flow rates in the range of 1–200 cm³/min; and a wet-test meter for flow rates greater than 200 cm³/min. Temperature controllers (Omega CN-9000) were used to con-

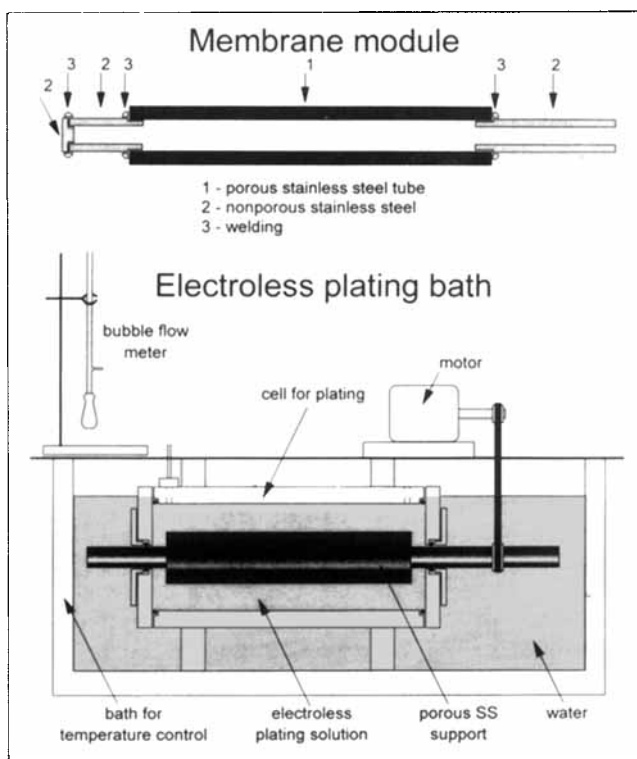


Figure 3. The membrane module and plating bath for the deposition of Pd on long porous stainless-steel tubes by the electroless-plating technique.

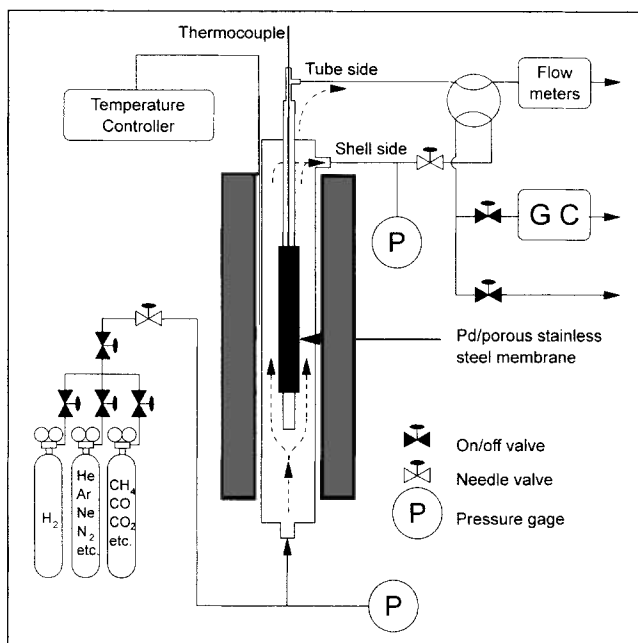


Table 3. Nitrogen Permeance of the Porous Stainless Steel

Sample No.	Treatment	Permeance (F), $\text{m}^3/(\text{m}^2 \cdot \text{h} \cdot \text{atm})$
1	None	230.4
1	Stainless-steel brush	182.1
1	+ Cleaning solution	206.5
1	+ 10 M HCl, 5 min	207.0
1	+ Activation ($\times 8$)	187.2
2	Sandpaper (intense)	49.4
2	+ Cleaning solution	71.0
2	+ 10 M HCl, 5 min	72.6
2	+ Activation ($\times 8$)	29.3
3	File (intense)	0.2
3	+ 10 M HCl, 20 h	112

Figure 5. Experimental setup for permeation measurements.

control the temperatures inside the furnace and inside the membrane module. The temperature variation along the membrane did not exceed 3°C .

To avoid hydrogen embrittlement the hydrogen fluxes were measured at temperatures greater than 300°C . Prior to the hydrogen permeation tests, the Pd/PSS membrane was heated in nitrogen or helium at a rate of about $1^\circ\text{C}/\text{min}$.

The fluxes of gases other than hydrogen (N_2 , Ar, CO_2 , CH_4 , CO, Ne, He) were measured following a thorough purge of both shell and tube sides by the permeating gas. Without purging, a negative flux would be observed as a result of back diffusion of the dissolved hydrogen.

All the gases used had 99.9% or better purity except carbon dioxide (99.8%).

Structural characterization

The microstructure of the membranes was characterized by scanning electron microscopy (SEM, JEOL-840) and X-ray diffraction (XRD, Rigaku/USA D/MAX APD System) with Cu K_α radiation sources and graphite monochromators.

Results and Discussion

Permeability of the original support

Dense Pd membranes were successfully prepared when a top layer of stainless steel was mechanically removed prior to cleaning, activation, and palladium deposition. The influence of different mechanical treatments on the permeation characteristics of the original PSS support was studied. It was found that conventional machining and mechanical treatments (sandpaper, file, etc.) of PSS closed surface pores decreased their size and, consequently, reduced the porosity of the top layer, making the treated surface almost impermeable. For example, the nitrogen permeance of the PSS long

tube dropped from ~ 200 to $0.2 \text{ m}^3/(\text{m}^2 \cdot \text{h} \cdot \text{atm})$ after surface filing (Table 3). Therefore, the controlled machining or mechanical treatment can be used to decrease the pore size of the top layer of the PSS support. Electrical discharge machining can keep the surface pores open without changes in the pore size (Mott Metallurgical, 1995). Treatment by a stainless-steel brush yielded a small reduction in the PSS permeability. A subsequent cleaning by alkaline solution in an ultrasonic bath increased the permeability of PSS to within 20% of the value prior to the brush treatment (Table 3). The simplicity of the treatment by stainless-steel brush, compared with electrical discharge machining, motivated the choice of this treatment.

Table 3 also shows that the short-term treatment by concentrated hydrochloric acid did not change the pore size and porosity of the PSS, while extended contact with the acid can reopen mechanically closed surface pores as a result of dissolving the top layer of stainless steel.

An activated layer, with a thickness of about $1 \mu\text{m}$, was responsible for the observed decrease in the PSS's permeability (Table 3). The change of the permeance was larger for #2, where the size of surface pores had been substantially decreased by the preliminary mechanical treatment.

Hydrogen flux and selectivity coefficient

The rate of hydrogen permeation or the hydrogen flux can be expressed as

$$J = \frac{Q}{L} \cdot (P^n - P_0^n) = F \cdot (P^n - P_0^n). \quad (1)$$

A typical relation with $n = 0.5$ between the rate of hydrogen permeation and the transmembrane pressure difference is shown in Figure 6. The hydrogen fluxes of 3.2 and $6.8 \text{ m}^3/(\text{m}^2 \cdot \text{h})$ at a pressure difference of 1 atm were measured at 350 and 500°C , respectively. These temperatures correspond to the permeances of 7.8 and $16.4 \text{ m}^3/(\text{m}^2 \cdot \text{h} \cdot \text{atm}^{0.5})$. The regression coefficient was usually around 0.999 for all the membranes tested (see Table 4). These results show that the dependence of the hydrogen solubility in Pd follows Sievert's law. Furthermore, the hydrogen diffusion through the bulk of the palladium film is the rate-determining step for hydrogen permeation.

An increase in the hydrogen flux can be achieved by decreasing the thickness of the palladium layer and increasing

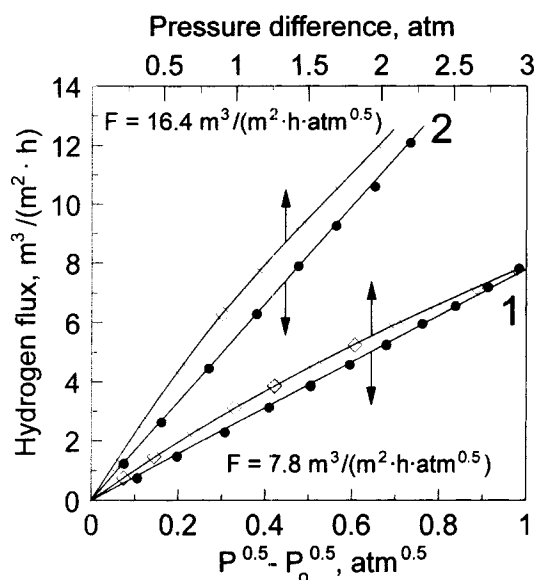


Figure 6. Influence of the pressure difference on the H₂ flux at (1) 350 and (2) 500°C.

the porosity of the support. The variation in the hydrogen fluxes with the porosity of the support for the same thickness of the Pd dense layer was discussed by Itoh et al. (1995). To deposit a thinner layer the pore size of the support should be smaller or should be decreased prior to the Pd deposition. Because of the differences between supports, such as effective porosity of the top layer and the diameter of the biggest pores, the thickness of Pd dense layer usually was varied from 19 to 28 μm and the hydrogen fluxes from 2 to 4 $\text{m}^3/(\text{m}^2 \cdot \text{h})$ were measured at a pressure difference of 1 atm. A thinner dense Pd layer also can be prepared by predominant deposition of palladium inside the pores of the top layer of the support.

Permeation of a wide range of pure gases through the Pd/PSS membranes was also studied. At room temperature nitrogen or helium fluxes through the freshly prepared membranes were not detected in many cases at pressure differ-

Table 4. Hydrogen Permeance and the Value of the Pressure Exponent from the Different Procedures of Estimation

Membr. No.	Permeat. Temp. °C	Type of Procedure to Estimate Value of n^*	n Pressure Exponent	Regress. Coeff.	Permeance $\text{m}^3/\text{m}^2 \cdot \text{hr} \cdot \text{atm}^n$
1	350	1	0.5	0.9991	7.934
		2	0.600	0.9998	6.220
		3	0.591	—	6.352
2	350	1	0.5	0.9993	3.928
		2	0.605	0.9999	3.036
		3	0.609	—	3.011
2	470	1	0.5	0.9985	7.1336
		2	0.646	0.9999	5.039
		3	0.635	—	5.158
2	500	1	0.5	0.9996	9.291
		2	0.434	0.9999	11.159
		3	0.443	—	10.856

* Procedure #1: $J = F \cdot (P^{0.5} - P_0^{0.5})$; procedure #2: $J = F \cdot (P^n - P_0^n) + B$; $\lim |B| \rightarrow 0$; procedure #3: $F = F_0 + A \cdot (P^n - P_0^n)$; $\lim |A| \rightarrow 0$.

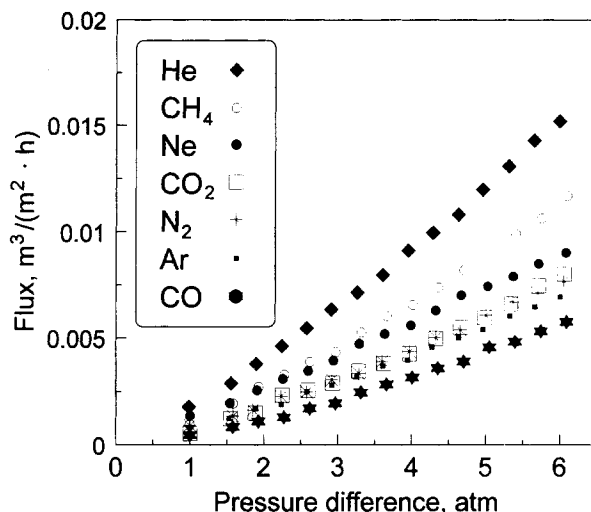


Figure 7. Flux of different gases as a function of the pressure difference at 350°C.

ence up to 3 atm. This strongly indicated that the deposited palladium layer was defect free and impermeable to any gas except hydrogen.

After increasing the temperature to 350°C in the nitrogen atmosphere, a very small nitrogen flux was detected. Figure 7 shows the fluxes of different gases other than hydrogen at 350°C as a function of the transmembrane pressure difference. Because of the very low permeability of the membrane for these gases, in many cases the fluxes could not be measured accurately at pressure differences less than 1 atm.

For all these gases, the fluxes increase exponentially with the pressure difference. Empirically, the fluxes could be described by Eq. 1, as has been done by Collins and Way (1993). They found that the exponent of the pressure, n , ranged from about 1.37 to 1.51 for helium and nitrogen. Another empirical way to express the variation of fluxes with the pressure difference is $J = F \cdot (P - P_0)^n$, with the value of n likewise being greater than 1.

There are at least two mechanisms involved in the transport process here: Knudsen diffusion and viscous or Poiseuille flow. For the Knudsen diffusion, permeance does not depend on the pressure difference, while for the viscous flow, the permeance should be proportional to the pressure. The viscous flow contribution is proportional to the average pressure across the membrane, which also determines the mean free path of the gas molecules. Therefore, for the same pressure difference, P_{ave} would be different for a different downstream pressure, P_0 . Thus, it appears that there is no real physical basis for presenting such fluxes either as $J = F \cdot (P^n - P_0^n)$ or as $J = F \cdot (P - P_0)^n$.

For nonadsorbable gases, the total permeance can be expressed as the sum of the Knudsen flow and the viscous or Poiseuille flow (Uhlhorn et al., 1989):

$$F = F_k + F_v \cdot P_{\text{ave}} = \frac{2}{3} \sqrt{\frac{8}{\pi}} \cdot \frac{\epsilon \mu_k r}{L \sqrt{RTM}} + \frac{1}{8} \cdot \frac{\epsilon \mu_v r^2}{L \eta RT} \cdot P_{\text{ave}} \quad (2)$$

The presence of surface flow should be taken into account if the pressure and temperature are such that gas adsorption

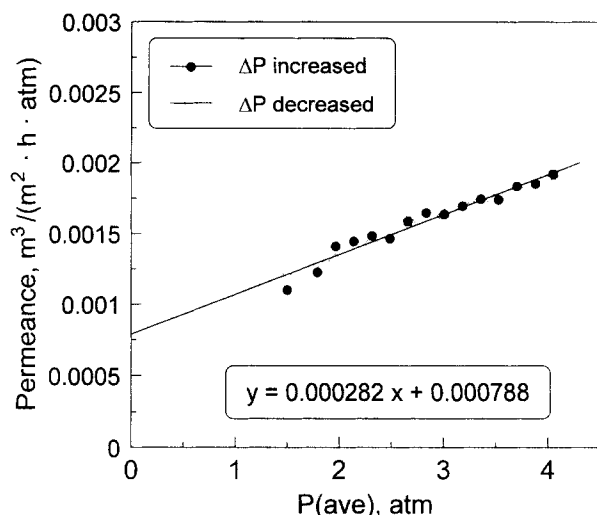


Figure 8. Methane permeance vs. average pressure across the membrane.

Circles: the pressure difference was consecutively increased; diamond: the pressure difference was consecutively decreased.

on the surface is significant. We can assume that for temperatures greater than 350°C, the contribution from the surface flow for He, Ne, Ar, N₂, CO₂, and CH₄ can be neglected. Equation 2 shows that a plot of F vs. P_{ave} should yield a straight line with the slope F_v and intercept F_k .

The permeances for all gases were plotted against the average pressure, P_{ave} , and the values of F_k and F_v were estimated. As an example, Figure 8 shows the methane permeation data as a function of the average pressure. To demonstrate the reproducibility of the permeation measurements, two sets of data are presented. The first (circles) illustrates the case where the pressure difference was consecutively increased from 1 to 6 atm, while the second set (diamonds) shows that the pressure was consecutively decreased in the same range of pressure differences. Since the data of both sets were so close, they were analyzed together. Intersection with axis Y gives the value of F_k , and the slope (F_v) indicates the contribution of the viscous flow to the total methane flow through the membrane. From Eq. 2 it can be seen that for a membrane at a given temperature, the F_k is inversely proportional to the square root of the molecular weight of the permeation gas, and F_v is inversely proportional to the viscosity of this gas at a given temperature.

The ideal separation factor, or selectivity coefficient (α^*), is defined as the ratio of the fluxes of two pure gases, i and j , as follows:

$$\alpha_{i/j}^* = \frac{J_i}{J_j} \quad (3)$$

The selectivity coefficients of gases—for example, argon—with respect to other gases, for pure Knudsen diffusion and for viscous flow, could be expressed by

$$\alpha_k^*(\text{Ar/gas}) = \frac{\sqrt{M_{\text{gas}}}}{\sqrt{M_{\text{Ar}}}} \quad (4)$$

and

$$\alpha_v^*(\text{Ar/gas}) = \frac{\eta_{\text{gas}}}{\eta_{\text{Ar}}} \quad (5)$$

respectively. The expected Ar selectivity coefficients for pure Knudsen diffusion, α_k^* , and for pure viscous flux, α_v^* , were calculated using Eqs. 4 and 5, respectively, and compared with the estimation from the experimental data as ratios $F_k(\text{Ar})/F_k(\text{gas})$ and $F_v(\text{Ar})/F_v(\text{gas})$, as shown in Figure 9a and 9b. The values of viscosity, η , for He, Ne, Ar, N₂, CO₂, and CH₄ at 350°C were calculated based on the data presented in the literature (Lide, 1996). The values of α_k^* and α_v^* obtained from the experimental data are very close to the values obtained from Eqs. 4 and 5.

The radius of pores can be approximately estimated based on the experimental ratio of F_v/F_k and on the assumption that the geometrical factors of a porous medium are the same for Knudsen diffusion and viscous flow:

$$\frac{F_v}{F_k} = \frac{3}{16} \sqrt{\frac{\pi}{8}} \cdot \frac{1}{\sqrt{RT}} \cdot \frac{\sqrt{M}}{\eta} \cdot r. \quad (6)$$

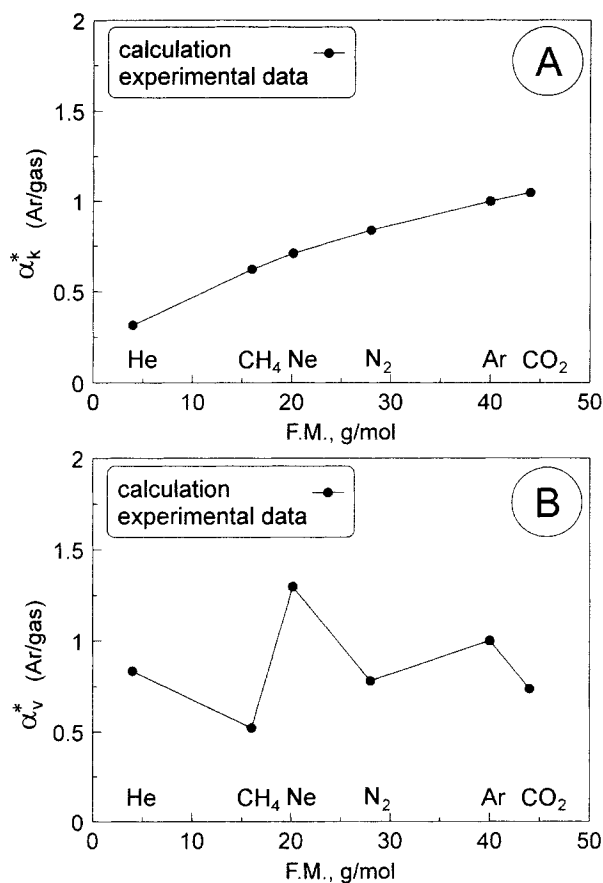


Figure 9. Expected selectivity coefficients (Ar/gas): (A) for pure Knudsen diffusion calculated from Eq. 4 vs. those estimated from experimental data as the ratio $F_k(\text{Ar})/F_k(\text{gas})$; (B) for pure viscous flux calculated from Eq. 5 with those estimated from the experimental data as the ratio of $F_v(\text{Ar})/F_v(\text{gas})$ $T = 350^\circ\text{C}$.

In the strict sense, the assumption that μ_k and μ_v are the same is not correct. The geometric factor μ_v is inversely related to tortuosity, τ : $\mu_v = 1/\tau$. The geometric factor for Knudsen diffusion includes not only tortuosity, but reflection factor, θ_k , as well: $\mu_k = 1/(\tau \cdot \theta_k)$. The reflection factor is proportional to the roughness of the wall of pores. For smooth walls, θ_k equals 1; for a rough surface, where the diffuse reflection of molecules takes place after collision with the wall, θ_k is greater than 1 (a detailed description of the geometric aspects can be found in Burggraaf, 1996). The exact value of τ should be θ_k times lower than that estimated from Eq. 6. At the same time, in our case, the roughness of the pore walls is determined by the roughness of the Pd grains, which is very low. The recrystallization texture and aggregation of the Pd grains is discussed later. It is then reasonable to assume that θ_k is close to 1 and $\mu_k \approx \mu_v = 1/\tau$. Thus, for $T = 350^\circ\text{C}$ Eq. 6 can be rewritten as

$$\frac{F_v}{F_k} = 1.632 \times 10^{-3} \cdot \frac{\sqrt{M}}{\eta} \cdot r. \quad (7)$$

As shown in Figure 10, a plot of the ratio of F_v/F_k vs. \sqrt{M}/η should be a straight line whose slope should yield the value of the pore radius, r , which in this case is $0.38 \mu\text{m}$. Considering the extremely low measured fluxes, it appears that the observed scattering of r is reasonable.

Using this average value of r , the porosity of the palladium layer was calculated as

$$\epsilon = 8 \cdot L \cdot \eta \cdot \tau \cdot RT \cdot F_v \cdot \frac{1}{r^2}. \quad (8)$$

The tortuosity factor, τ , is most likely to be between 3 and 4. Therefore, a value of 3.5 was used in the calculations. From the value of porosity and assuming a uniform distribution and cylindrical shaped pores, the number of pores (N) per unit area (S) and the distance between their centers (l) were calculated according to

$$N = \frac{\epsilon \cdot S}{\pi r^2} \quad (9)$$

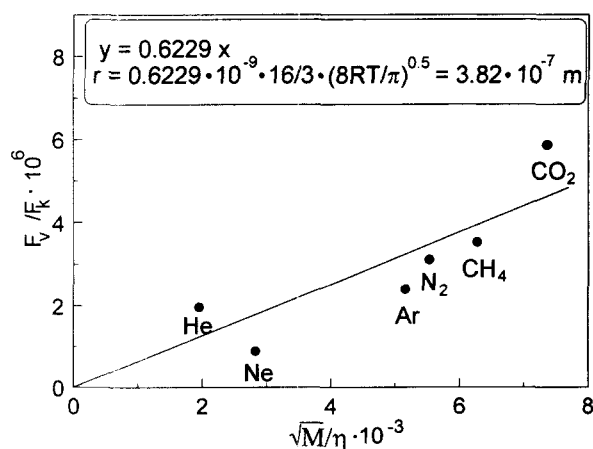


Figure 10. Variation of the ratio F_v/F_k as a function of \sqrt{M}/η .

$$l = \frac{\sqrt{S}}{\sqrt{N}}. \quad (10)$$

The calculated values of ϵ , N , and l are 1.79×10^{-7} , 0.39 per 1 mm^2 , and 1.61 mm , respectively.

The number of holes or pore entrances in the top layer of the PSS, which have an average diameter of $20\text{--}30 \mu\text{m}$ shown in Figure 1, is around 40 ± 10 per 1 mm^2 . To estimate the dimension of the pores and the pore-size distribution on the outer surface of the original PSS, computer-controlled scanning electron microscopy (CCSEM, RJ Lee Group, Inc., 530 McCormick St., San Leonardo, CA) was used. In CCSEM the backscattered electron mode, which is sensitive to differences in atomic number, is used to determine when the electron beam is in the pore. When a pore is located, the computer drives the beam in a preset pattern to determine the dimensions of the pore. The measurements performed by the RJ Lee Group indicated that the largest pores, with a diameter in the range between 7 and $8 \mu\text{m}$, made up about 1% of all pores. Based on the assumption of a uniform distribution of pores, therefore, we can conclude that the number of pores with large openings ($20\text{--}30 \mu\text{m}$) at one end (at the surface of PSS), but narrowing to $7\text{--}8 \mu\text{m}$ at the other end, is roughly 0.4 ± 0.1 per 1 mm^2 . This is in good agreement with the value of N , 0.39 per 1 mm^2 , calculated from Eq. 9. Thus, the pore gaps generated in the Pd layer while heating the membrane to 350°C are more likely to be located above such pores. Excessive tension exists in the Pd layer at points above these pores at high temperatures and causes the appearance of pore gaps, which reduce this tension. To decrease the probability of the creation of pore gaps, a thicker Pd layer should be deposited, or the pore entrances, as well as the large pores, should be blocked prior to the activation and deposition. Another way to prevent the creation of pore gaps is, as was mentioned before, the deposition of predominantly Pd inside the pores of the top layer.

Since the pressure dependence of the hydrogen flux is different from all other gases, the selectivity coefficient between

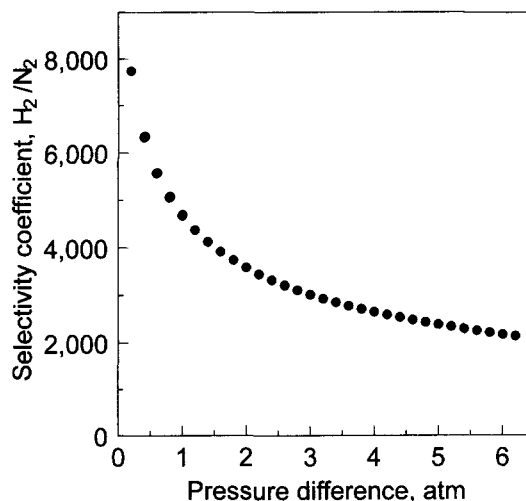


Figure 11. H_2/N_2 selectivity coefficient as a function of the pressure difference at 350°C (based on the experimental data).

hydrogen and other gases depends on the pressure differences, as shown in Figure 11 for nitrogen. The H_2/N_2 selectivity coefficients for other prepared membranes at 350°C and a pressure difference of 1 atm, ranged from 600 to 5,000.

Temperature dependence of membrane performance

Figure 12 shows a variation of the hydrogen and nitrogen fluxes with the temperature at pressure differences of 0.5, 1, 1.5 and 2 atm. In this experiment the temperature was increased from 350°C to 700°C and the membrane was held at each temperature for about 5 h. Temperatures greater than 700°C were not applied due to the large reduction in hydrogen flux and the considerable increase in nitrogen flux.

For such a membrane temperature history, the permeation data reflect the influence of the temperature on both fluxes and the reorganization of the membrane structure. As expected, an increase in temperature leads to an increase in hydrogen flux. The drop in fluxes at temperatures greater than 550°C was most likely caused by an intermetallic diffusion. At temperatures greater than 550°C similar deterioration in the hydrogen permeation rate was observed for all membranes prepared in this manner.

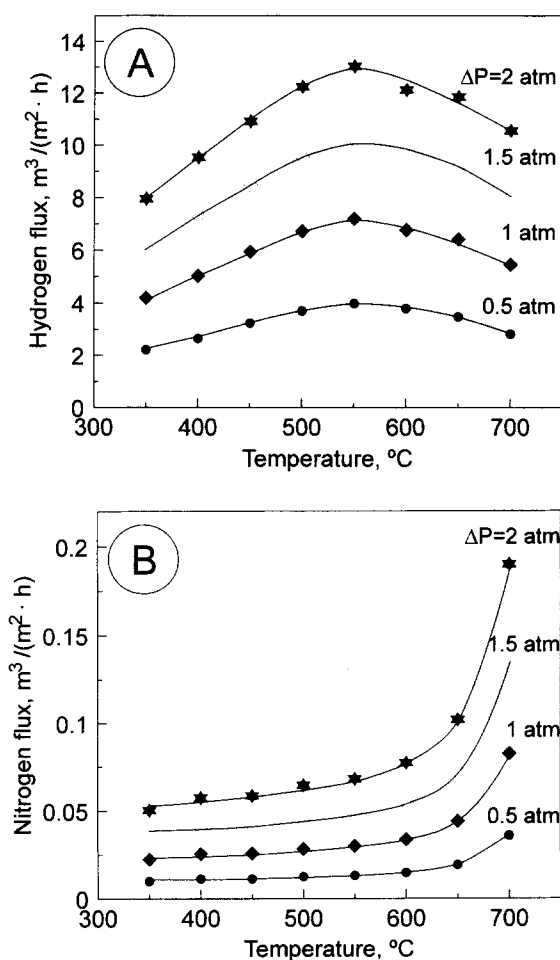


Figure 12. Influence of temperature on H_2 (A) and N_2 (B) fluxes for different ΔP ; temperature was increased from 350°C to 700°C.

The value of the exponent of the pressure, n , is routinely used as an indication of the rate-limiting step of the hydrogen permeation through the Pd layer. If the value of n is equal to 0.5, Sievert's law is assumed to be followed (Hurlbert and Konecny, 1961). An increase in n will result when the permeation rate is influenced by the surface process, leakage of the hydrogen through defects in the Pd layer, transport resistance of the support, poisoning of the palladium surface, and so forth. Collins and Way (1993) mentioned that n also depends on the temperature. The same assumption was made by Hurlbert and Konecny (1961). They found that for the palladium film with thickness $\geq 20 \mu m$ and at 350°C the value of n is 0.68, and they concluded that with increasing temperature, the value of n should probably decrease to the limiting value 0.5.

The value of n , which best fits the permeation data, was estimated. Two procedures are commonly used to estimate the optimum value of n : J is plotted against $(P^n - P_0^n)$, $J = F \cdot (P^n - P_0^n) + B$, $\lim_{|B| \rightarrow 0} B \rightarrow 0$; and F is plotted against $(P^n - P_0^n)$, $F = F_0 + A \cdot (P^n - P_0^n)$, $\lim_{|A| \rightarrow 0} A \rightarrow 0$. It was found that in some cases the optimum value of n was indeed lower at higher temperatures, as was mentioned by Hurlbert and Konecny (1961) and Collins and Way (1993), but such a correlation was not always valid. As an example, Table 4 gives n , F , and regression coefficient, R^2 , for different membranes at different temperatures of measurements (the differences in permeances are mainly due to the different quality of the support). The goodness of fit is relatively insensitive to the value of n . A good fit does not necessarily prove that this value of n reflects the quality of the membrane or could be used to reach a conclusion about the rate-limiting step of the hydrogen permeation, especially if the value is in the range between 0.4 and 0.6. Therefore, the optimum value of n is too sensitive to the accuracy of the permeation measurements to be used without a great care.

Significant increases in the pressure exponent up to 0.8–0.9 were observed only at the temperatures around 700°C. This increase in n was caused by the degradation of the membrane and accompanied by a 4-fold increase of the nitrogen flux. The increase of the nitrogen flux with the temperature (Figure 12b), contrary to the theory (Eq. 2), was due to the modification of the morphology of the Pd layer.

Intermetallic diffusion is a severe problem for the application of the palladium membranes at high temperatures because of the decline of the hydrogen flux. It is well known that a considerable thermal vibration occurs in the metal lattice at the Tamman temperature that is equal to 0.5 of its melting temperature (in K). If there is an interface between two metals, this thermal vibration enormously increases the mobility of metal atoms and their capability for diffusion. Palladium and stainless steel have melting points of 1,552 and 1,375–1,400°C, respectively. The corresponding Tamman temperatures are about 640 and 550–560°C. We could therefore expect that at temperatures around 550°C the diffusion of stainless-steel components into the palladium layer should take place. An alloy of Pd with the SS components created under such circumstances would have lower hydrogen fluxes. This reasoning is in very good agreement with the data presented in Figure 12a. Moreover, Gryaznov et al. (1993) showed by XPS that stainless-steel components indeed diffused into the palladium layer. Thus, the lowest Tamman

temperature of the metal-metal couple determines the temperature where substantial intermetallic diffusion occurs.

One way to prevent such diffusion is the creation of an additional thermostable oxide layer between the Pd layer and the support. Edlund and Pledger (1993) successfully prepared composite membrane Pd/SiO₂/V/SiO₂/Pt, which maintained good thermal stability. Edlund and McCarthy (1995) later reported membrane stability for up to 80 h at 700°C for their composite Pd/V membrane with nonwoven aluminum oxide felt as an intermediate layer. Gryaznov et al. (1993) showed that the best resistance to intermetallic diffusion between PSS and Pd, deposited by magnetron sputtering, are zirconia, magnesia, tantalum oxide, and tungsten. Tungsten can be used as an intermediate layer because of its extremely high melting temperature and, consequently, high Tamman temperature of about 1,570°C.

If the membrane has been treated at high temperatures prior to the permeation experiments, and the temperature did not exceed the temperature of intermetallic diffusion, the measured fluxes of hydrogen and nitrogen depended only on the temperature. Under the current condition the membrane performance should not be affected by the reorganization of the palladium layer. The hydrogen and nitrogen flux as a function of the temperature for the membrane initially treated

at 500°C for 5 h is presented in Figure 13. In agreement with the theory, the nitrogen flux decreases as the temperature increases. The increase in the hydrogen flux and the decrease in the nitrogen flux with temperature result in an increase in the selectivity coefficient at high temperatures. According to the data presented in Figure 13, at 1-atm pressure difference the selectivity coefficient changed from 1,390 at 350°C to 3,350 at 470°C.

The experimental values of the hydrogen permeances at different temperatures were used to estimate the activation energy for hydrogen permeation through the membrane. The permeability depends on the temperature, as

$$Q = Q_0 \cdot \exp\left(-\frac{E}{RT}\right). \quad (11)$$

This equation is correct when the value of n does not depend on the temperature. For all temperatures $n = 0.5$ was used. Figure 14 shows an Arrhenius relation between the rate of hydrogen permeance and the temperature. The activation energy of the composite membrane for hydrogen permeation, calculated from this graph, is 16.4 kJ/mol. Similar activation energy of 19.7 kJ/mol was reported earlier (Mardilovich et al., 1996b) for a different membrane. These values are in agreement with those for Pd membranes reported previously: 14.45 kJ/mol for 17 μm Pd film on ceramic support (Collins and Way, 1993); and 23 kJ/mol for 0.3 μm Pd/Ag film on ceramic support (Jayaraman and Lin, 1995). In the later case, since a hydrogen-to-nitrogen selectivity coefficient as low as 5.7 was reported, it is difficult to assess the quality of the membrane. Furthermore, the hydrogen fluxes were studied only in the range of temperature from 100 to 250°C.

Long-term stability

Pd/PSS membranes must demonstrate long-term stability if they are to be viable for industrial applications. The membranes were tested at 350°C for up to 1100 h. Figure 15 shows permeation measurements through the membrane at 350°C

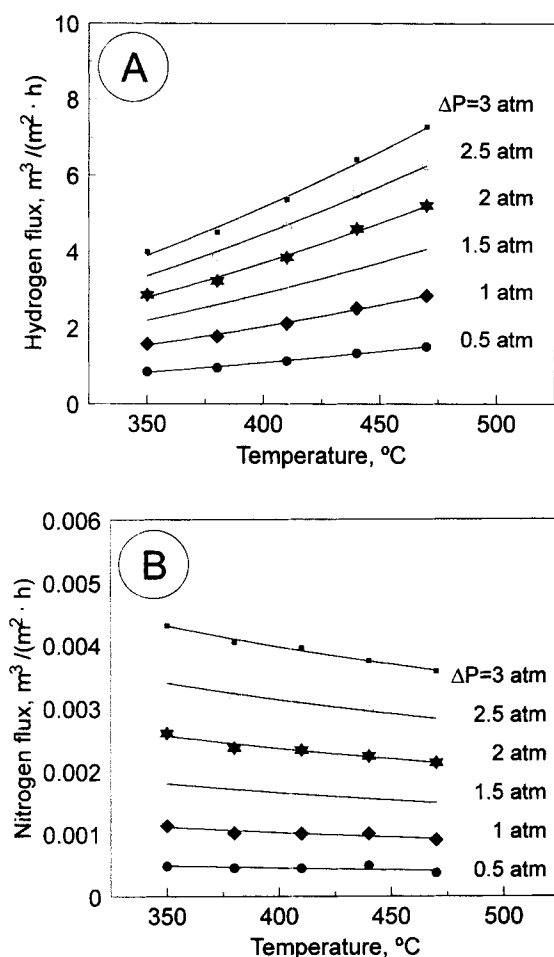


Figure 13. Influence of temperature on H₂ (A) and N₂ (B) fluxes for different ΔP ; temperature was decreased from 500°C to 350°C.

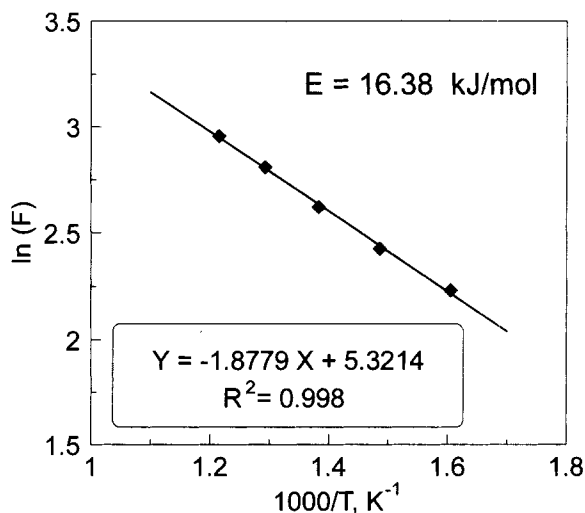


Figure 14. Arrhenius relation between the hydrogen permeance and the temperature.

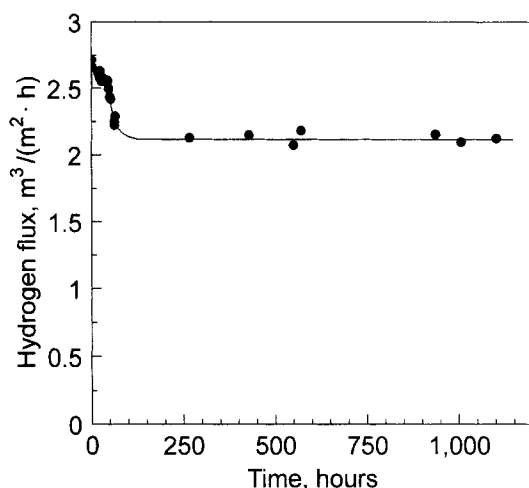


Figure 15. Hydrogen flux vs. time: $P = 2$ atm; $P_0 = 1$ atm; $T = 350^\circ\text{C}$.

over a period of 1,100 h. During this period of time the hydrogen partial pressure difference varied from 0.1 to 6 atm and fluxes of many other gases and mixtures, such as N_2 , Ar, He, CO_2 , CH_4 , N_2/H_2 , CO_2/H_2 , were also measured. No significant changes of the membrane performance were observed, except for the initial decrease of the hydrogen flux. The decline in the hydrogen flux over the first ~ 50 h is more likely the result of rearrangement of the Pd/PSS interface with the rest of the activated layer. Under high temperatures and in the presence of hydrogen this layer becomes denser and the local, effective porosity of the support's top layer is decreased, resulting in the loss of effective membrane area.

Figure 16 shows SEM photographs of Pd/PSS membranes exposed at 350°C for 5 and 1,100 h. After 1,100 h, the distribution of the Pd crystal orientation is nonrandom. From the XRD data presented in Figure 17, it can be seen that the preferred orientation is (111). A recrystallization texture has been developed by a recrystallization process that is also accompanied by the aggregation of grains. After 1,100 h at 350°C , some of the grains are as large as $5\ \mu\text{m}$. According to the XRD data the size of the initial Pd grains just after deposition is around 20 nm (calculations were made by JADE software, MDI Material Data Inc., using the Debye-Scherrer equation). Treatment of the Pd/PSS membrane at 700°C leads to the additional reorganization of the palladium texture. Figure 17 shows that the Pd membrane treated at 700°C has a predominantly (200) crystal orientation.

The Pd lattice parameter, a_0 , was found to be $3.887\ \text{\AA}$, $3.894\ \text{\AA}$, $3.893\ \text{\AA}$, and $3.894\ \text{\AA}$ for the original membrane, the membrane treated at 350°C for 5 and 1100 h, and the membrane treated at 700°C for 5 h, respectively. Lattice parameters were estimated by plotting the value of a , calculated for each reflection at 2θ up to 130° , against $\sin^2\theta$ and extrapolation to a value a_0 at $\theta = 90^\circ$ (Cullity, 1988). The recrystallization of the deposited palladium at 350°C , and the treatment at 700°C do not appear to lead to any significant changes of the lattice. The parameters for Pd treated at 350°C and higher are very close to the a_0 for pure Pd as reported in the literature ($a_0 = 3.8898\ \text{\AA}$; Berry, 1974) and to that estimated in

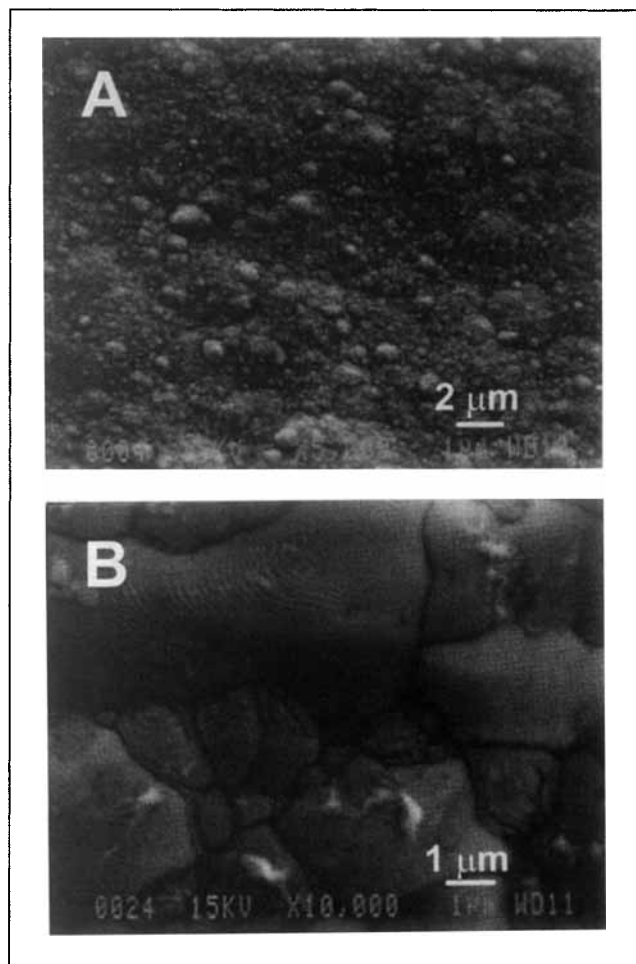


Figure 16. Surface morphology of the Pd/porous stainless-steel membrane after exposure at 350°C for (A) 5 and (B) 1,100 h.

this study using a Pd sheet ($a_0 = 3.891\ \text{\AA}$; XRD pattern of Pd sheet presented in Figure 17, curve 5).

Based on the data presented here and in the previous paragraph, we can conclude that the prepared membranes can withstand brief operation at temperatures up to 500 – 550°C . For long-term exposures, a more appropriate temperature range is from around 300°C to 450°C . The minimum operating temperature of 300°C for pure Pd is defined by hydrogen embrittlement, a phenomenon when the β palladium hydride may nucleate from the α phase. This causes loss in density in the Pd layer and the selectivity of the membrane as a result of alternative Pd lattice expansion and reduction (Saracco and Specchia, 1994; Shu et al., 1991).

Conclusions

The results of this research show that the electroless plating technique can produce a dense Pd layer on long, porous stainless-steel tubes with pores up to $8\ \mu\text{m}$. At room temperature the nitrogen or the helium fluxes through such membranes were not detected at pressure differences up to 3 atm. The thickness of the dense Pd layer strictly depended on the diameter of the largest pores in the support.

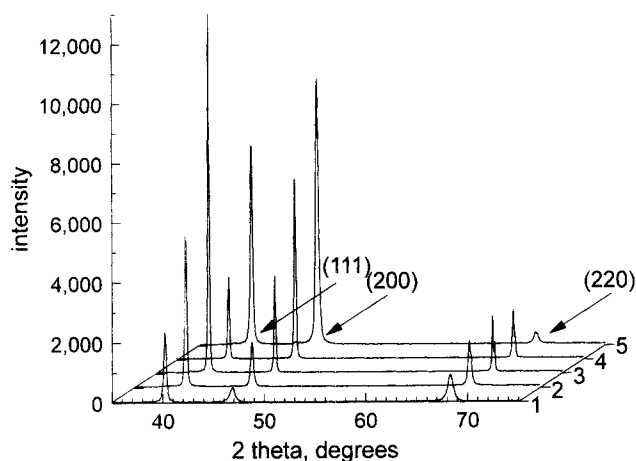


Figure 17. XRD of the initial Pd/porous stainless-steel membrane (1); membrane after exposure at 350°C for 5 h (2) and 1,100 h (3); after exposure at 700°C for 5 h (4), and a sheet of pure Pd (5).

At 350°C the developed membranes with a palladium layer of $\sim 20 \mu\text{m}$ exhibited hydrogen permeances up to $8 \text{ m}^3/(\text{m}^2 \cdot \text{h} \cdot \text{atm}^{0.5})$. At a pressure difference of 1 atm and 350°C selectivity coefficients (H_2/N_2) as high as 5000 and hydrogen fluxes up to $4 \text{ m}^3/(\text{m}^2 \cdot \text{h})$ were observed. The selectivity coefficient rose with the temperature increase and the decrease in pressure difference.

The contribution of viscous flux was taken into account to explain the transport mechanism of gases other than hydrogen through the membranes. It was found that these gases pass through the pore gaps in the palladium layer. These pore gaps are most likely created during thermal treatment to reduce the excessive tension at the points located above the 7–8- μm pores with large (20–30 μm) openings at the surface of the PSS. Their low-density (less than $1 \text{ per } 1 \text{ mm}^2$) gives low values of the permeance through the gaps [around $0.001 \text{ m}^3/(\text{m}^2 \cdot \text{h} \cdot \text{atm})$]. These fluxes could be decreased further by the deposition of a thicker Pd layer or by partial blocking of the big PSS pores prior to activation and deposition.

The long exposure (1,100 h and more) of the membrane to hydrogen at 350°C led to the recrystallization texture. The (111) orientation became preferred, and aggregation of the palladium grains occurred. The hydrogen flux did not vary significantly in time. At temperatures of 550°C and higher, the membranes could withstand only brief operation without appreciable changes in the hydrogen flux and selectivity, because of the intermetallic diffusion.

The Pd membranes that were developed show themselves to be extremely promising for practical applications in the range of temperatures from ~ 300 to 450°C.

Acknowledgment

We gratefully acknowledge the financial support provided by China Technical Consultants, Inc., Taipei, Taiwan, R.O.C.

Notation

E = activation energy, J/mol

F = rate of gas permeation per unit area and per unit of a trans-membrane pressure difference, or permeance, $\text{mol}/(\text{m}^2 \cdot \text{s} \cdot \text{Pa})$ or $\text{m}^3/(\text{m}^2 \cdot \text{h} \cdot \text{atm})$

F_k = permeance due to Knudsen diffusion, $\text{mol}/(\text{m}^2 \cdot \text{s} \cdot \text{Pa})$

F_v = permeance divided by pressure due to viscous or Poiseuille flow, $\text{mol}/(\text{m}^2 \cdot \text{s} \cdot \text{Pa}^2)$

J = rate of gas permeation per unit area, or flux, $\text{mol}/(\text{m}^2 \cdot \text{s})$ or $\text{m}^3/(\text{m}^2 \cdot \text{h})$

L = thickness of the Pd layer, m

M = molecular mass of the gas, kg/mol or g/mol

P = upstream pressure, Pa or atm

R = gas constant, J/mol \cdot K ($= 8.315$)

Literature Cited

- Athayde, A. L., R. W. Baker, and P. Nguyen, "Metal Composite Membranes for Hydrogen Separation," *J. Memb. Sci.*, **94**, 299 (1994).
- Berry, L. G., ed., *Powder Diffraction File*, 4-783 and 5-0681, Joint Committee of Powder Diffraction Standards, PA (1974).
- Bryden, K. J., and J. Y. Ying, "Nanostructured Palladium Membrane Synthesis by Magnetron Sputtering," *Mater. Sci. Eng.*, **A204**, 140 (1995).
- Burggraaf, A. J., "Transport and Separation Properties of Membranes with Gases and Vapors," *Fundamentals of Inorganic Membrane Science and Technology*, A. J. Burggraaf and L. Cot, eds., Elsevier, Amsterdam, The Netherlands, p. 331 (1996).
- Buxbaum, R. E., and T. L. Marker, "Hydrogen Transport Through Non-porous Membranes of Palladium-Coated Niobium, Tantalum and Vanadium," *J. Memb. Sci.*, **85**, 29 (1993).
- Buxbaum, R. E., and A. B. Kinney, "Hydrogen Transport Through Tubular Membranes of Palladium-Coated Tantalum and Niobium," *Ind. Eng. Chem. Res.*, **35**, 530 (1996).
- Collins, J. P., and J. D. Way, "Preparation and Characterization of a Composite Palladium-Ceramic Membrane," *Ind. Eng. Chem. Res.*, **32**, 3006 (1993).
- Cullity, B. D., *Elements of X-Ray Diffraction*, Addison-Wesley, Reading, MA (1978).
- Edlund, D. J., and J. McCarthy, "The Relationship Between Inter-metallic Diffusion and Flux Decline in Composite-Metal Membranes: Implications for Achieving Long Membrane Lifetime," *J. Memb. Sci.*, **107**, 147 (1995).
- Edlund, D. J., and W. A. Pledger, "Thermolysis of Hydrogen Sulfide in a Metal-Membrane Reactor," *J. Memb. Sci.*, **77**, 255 (1993).
- Govind, R., and D. Atnoor, "Development of a Composite Palladium Membrane for Selective Hydrogen Separation at High Temperature," *Ind. Eng. Chem. Res.*, **30**, 591 (1991).
- Gryaznov, V. M., O. S. Serebryannikova, M. Yu. Serov, M. M. Ermilova, A. N. Karavanov, A. P. Mischenko, and N. V. Orekhova, "Preparation and Catalysis over Palladium Composite Membranes," *Appl. Catal. A: General*, **96**, 15 (1993).
- Honma, H., and K. Kanemitsu, "Electroless Nickel Plating on Alumina Ceramics," *Plat. Surf. Finish.*, 62 (1987).
- Hurlbert, R. C., and J. O. Konecny, "Diffusion of Hydrogen through Palladium," *J. Chem. Phys.*, **34**, 655 (1961).
- Hybertson, B. M., B. N. Hansen, R. M. Barkley, and R. E. Sievers, "Deposition of Palladium Films by a Novel Supercritical Fluid Transport-Chemical Deposition Process," *Mater. Res. Bull.*, **26**, 1127 (1991).
- Itoh, N., T.-H. Wu, and K. Haraya, "Two- and Three-Dimensional Analysis of Diffusion Through a Dense Membrane Supported on a Porous Material," *J. Memb. Sci.*, **99**, 175 (1995).
- Jayaraman, V., and Y. S. Lin, "Synthesis and Hydrogen Permeation Properties of Ultrathin Palladium-Silver Alloy Membranes," *J. Memb. Sci.*, **104**, 251 (1995a).
- Jayaraman, V., Y. S. Lin, M. Pakala, and R. Y. Lin, "Fabrication of Ultrathin Metallic Membranes on Ceramic Supports by Sputter Deposition," *J. Memb. Sci.*, **99**, 89 (1995b).
- Kikuchi, E., and S. Uemiyu, "Preparation of Supported Thin Palladium-Silver Alloy Membranes and Their Characteristics for Hydrogen Separation," *Gas Sep. Purif.*, **5**, 261 (1991).
- Konno, M., M. Shindo, S. Sugawara, and S. Saito, "A Composite Palladium and Porous Aluminum Oxide Membrane for Hydrogen Gas Separation," *J. Memb. Sci.*, **37**, 503 (1988).

- Li, Z. Y., H. Maeda, K. Kusakabe, S. Morooka, H. Anzai, and S. Akiyama, "Preparation of Palladium-Silver Alloy Membranes for Hydrogen Separation by the Spray Pyrolysis Method," *J. Memb. Sci.*, **78**, 247 (1993).
- Lide, D. R., ed., *Handbook of Chemistry and Physics*, 77th ed., CRC Press, Boca Raton, FL (1996).
- Mardilovich P. P., P. V. Kurman, A. N. Govyadinov, I. P. Mardilovich, M. M. Ermilova, N. V. Orekhova, A. N. Krivoshanova, R. Paterson, and V. M. Gryaznov, "Gas Permeability of Anodized Alumina Membranes with a Palladium-Ruthenium Alloy Layer," *Russ. J. Phys. Chem.*, **70**, 514 (1996a).
- Mardilovich, P. P., Y. She, M.-H. Rei, and Y. H. Ma, "Permeation Characterization of Defect Free Pd/Porous Stainless Steel Membranes," Int. Conf. on Inorganic Membranes, Gatlinburg, TN (1996b).
- McBride, R. B., and D. L. McKinley, "A New Hydrogen Recovery Route," *Chem. Eng. Progr.*, **61**(3), 81 (1965).
- Melashchenko, N. F., *Galvanic Coatings of Dielectrics*, Belarus, Minsk (1987).
- Morooka, S., S. Yan, S. Yokoyama, and K. Kusakabe, "Palladium Membrane Formed in Macropores of Support Tube by Chemical Vapor Deposition with Crossflow Through a Porous Wall," *Sep. Sci. Technol.*, **30**, 2877 (1995).
- Mott Metallurgical Corporation or Newmet Krebsoge, Inc., Manufacturer literature, (1995).
- Peachey, N. M., R. C. Snow, and R. C. Dye, "Composite Pd/Ta Metal Membranes for Hydrogen Separation," *J. Memb. Sci.*, **111**, 123 (1996).
- Saracco, G., and V. Specchina, "Catalytic Inorganic-Membrane Reactors: Present Experience and Future Opportunities," *Catal. Rev.-Sci. Eng.*, **36**(2), 305 (1994).
- Shu, J., B. P. A. Grandjean, A. Van Neste, and S. Kaliaguine, "Catalytic Palladium-Based Membrane Reactors: Review," *Can. J. Chem. Eng.*, **69**, 1036 (1991).
- Shu, J., B. P. A. Grandjean, E. Ghali, and S. Kaliaguine, "Simultaneous Deposition of Pd and Ag on Porous Stainless Steel by Electroless Plating," *J. Memb. Sci.*, **77**, 181 (1993).
- Uemiyama, S., Y. Kude, K. Sugino, N. Sato, T. Matsuda, and E. Kikuchi, "A Palladium/Porous-Glass Composite Membrane for Hydrogen Separation," *Chem. Lett.*, **10**, 1687 (1988).
- Uemiyama, S., N. Sato, H. Ando, Y. Kude, T. Matsuda, and E. Kikuchi, "Separation of Hydrogen Through Palladium Thin Film Supported on a Porous Glass Tube," *J. Memb. Sci.*, **56**, 303 (1991a).
- Uemiyama, S., T. Matsuda, and E. Kikuchi, "Hydrogen Permeable Palladium-Silver Alloy Membrane Supported on Porous Ceramics," *J. Memb. Sci.*, **56**, 315 (1991b).
- Uhlhorn, R. J. R., K. Keizer, and A. J. Burggraaf, "Gas and Surface Diffusion in Modified γ -Alumina Systems," *J. Memb. Sci.*, **46**, 225 (1989).
- Yan, S., H. Maeda, K. Kusakabe, and S. Morooka, "Thin Palladium Membrane Formed in Support Pores by Metal-Organic Chemical Vapor Deposition Method and Application to Hydrogen Separation," *Ind. Eng. Chem. Res.*, **33**, 616 (1994).
- Yeung, K. L., and A. Varma, "Novel Preparation Techniques for Thin Metal-Ceramic Composite Membranes," *AIChE J.*, **41**, 2131 (1995).
- Yeung, K. L., R. Aravin, J. Szeigner, and A. Varma, "Metal Composite Membranes: Synthesis, Characterization and Reaction Studies," *Stud. Surf. Sci. Catal.*, **101**, 1349 (1996).

Manuscript received June 30, 1997, and revision received Sept. 29, 1997.